JOURNAL OF GEOPHYSICAL RESEARCH, VOL. 100, NO. D1, PAGES 1389–1396, JANUARY 20, 1995

Phase equilibria of H_2SO_4, HNO_3, and HCl hydrates and the composition of polar stratospheric clouds

Paul J. Wooldridge, Renyi Zhang,[1] and Mario J. Molina

Department of Earth, Atmospheric and Planetary Sciences and Department of Chemistry
Massachusetts Institute of Technology, Cambridge

Abstract. Thermodynamic properties and phase equilibria behavior for the hydrates and coexisting pairs of hydrates of common acids which exist in the stratosphere are assembled from new laboratory measurements and standard literature data. The analysis focuses upon solid-vapor and solid-solid-vapor equilibria at temperatures around 200 K and includes new calorimetric and vapor pressure data. Calculated partial pressures versus $1/T$ slopes for the hydrates and coexisting hydrates agree well with experimental data where available.

Introduction

The depletion of ozone in the polar stratosphere is generally accepted to be initiated by heterogeneous processes occurring on particulate surfaces [e.g., *Solomon*, 1988; *Molina*, 1991, 1994]. These processes repartition chlorine from relatively inert and photostable "reservoir" compounds (principally HCl and $ClONO_2$) to more photolabile forms (Cl_2, HOCl) which are easily converted into the chlorine radicals (Cl, ClO), resulting in catalytic ozone destruction. Also key to extensive ozone destruction is the concomitant "denoxification," that is, the repartitioning of nitrate species (NO_x) from the gas phase to the solid phase, where they are unavailable to decrease the chlorine radical concentrations by reforming the $ClONO_2$ reservoir species.

Polar stratospheric clouds (PSCs) are broadly classified as being either type I, generally assumed to be crystals of nitric acid trihydrate (NAT), or type II, which are composed of ordinary ice [*Toon et al.*, 1986; *Crutzen and Arnold*, 1986; *McElroy et al.*, 1986]. On the other hand, the background "sulfate aerosol" of the midlatitude lower stratosphere consists of 60–80 wt % H_2SO_4 aqueous solutions [e.g., *Turco et al.*, 1982]. Recent investigations have revealed that upon cooling to temperatures characteristic of the lower polar stratosphere (190–200 K), sulfuric acid droplets will swell not only from absorbing additional water vapor but also take up appreciable amounts of nitric acid from the gas phase and, upon continued cooling, become highly supercooled sulfuric acid/nitric acid/water droplets [*Zhang et al.*, 1993a] which crystallize at temperatures close to the ice frost point, eventually producing NAT and H_2SO_4 hydrates [*Molina et al.*, 1993; *Beyer et al.*, 1994].

In addition to ice and NAT, liquid and frozen sulfuric acid solutions have been shown to efficiently catalyze chlorine activation reactions at sufficiently low stratospheric temperatures [*Molina et al.*, 1993; *Hanson and Ravishankara*, 1993; *Zhang et al.*, 1994]. Furthermore, liquid aerosol droplets participate in ozone destruction by enhancing the repartitioning of oxidized nitrogen species via the heterogeneous reaction $N_2O_5 + H_2O \rightarrow HNO_3$, which occurs throughout most of the lower stratosphere [*Kolb et al.*, 1995].

Our knowledge of the physical properties and chemistry of these aqueous acids and their crystalline hydrates at low temperatures has greatly improved since the discovery of the Antarctic ozone hole. Vapor pressure measurements under conditions representative of the lower stratosphere have been carried out for the HNO_3/H_2O [*Hanson and Mauersberger*, 1988a, b; *Worsnop et al.*, 1993], the HCl/H_2O [*Hanson and Mauersberger*, 1990; *Abbatt et al.*, 1992], and the H_2SO_4/H_2O binary systems [*Zhang et al.*, 1993b]. *Smith* [1990] commented on the general thermodynamic consistency between HNO_3/H_2O solid-vapor phase diagrams generated from vapor pressure measurements and that expected from the standard thermodynamic properties of that binary system [*Forsythe and Giauque*, 1942]. In addition, thermodynamic data from various sources have been correlated and parameterized for the H_2SO_4/H_2O [e.g., *Zeleznik*, 1991] and HNO_3/H_2O [*Clegg and Brimblecombe*, 1990] binary systems.

The acids considered here are H_2SO_4, HNO_3, and HCl. On a molecule-per-molecule basis, bromine species are much more efficient in catalytic ozone destruction than those of chlorine, but atmospheric HBr mixing ratios are too small for significant amounts to be present in the condensed phase. The concentration of HF in the stratosphere is comparable to that of HCl; however, its hydrates are expected not to be stable under stratospheric conditions. They will likely have high HF vapor pressures as their stoichiometries are $H_2O \cdot n\text{HF}$, with $n \geq 1$ [*Cady and Hildebrand*, 1930], rather than acid $\cdot\, nH_2O$ as in the cases considered here.

In this report we summarize phase equilibria of the individual hydrates as well as coexisting pairs of hydrates, with emphasis on the boundaries of the stability regimes, as predicted from literature thermodynamic data and in some instances augmented with new data from our laboratory. These include measurements of vapor pressures over coexisting pairs of hydrates by mass spectrometry and determinations of the heats of fusion for the lesser studied hydrates $HCl \cdot 6H_2O$ and $HNO_3 \cdot 2H_2O$ by differential scanning calorimetry.

[1]Now at the Jet Propulsion Laboratory, California Institute of Technology, Pasadena.

Paper number 94JD02745.
0148-0227/95/94JD-02745$05.00

Methodology for Solid-Vapor Equilibrium

Consider the generalized binary process for two gaseous species forming a solid product C

$$v_A A + v_B B \Leftrightarrow C, \tag{1}$$

in which A and B are the gaseous components and the v_i are integers that define the stoichiometry. The partial pressures of A and B, p_A and p_B, are related by the equilibrium constant K_p for this process [e.g., *Denbigh*, 1981, section 4.12]

$$K_p = p_A^{v_A} p_B^{v_B}, \tag{2}$$

which is a function only of temperature. Second-order effects such as those arising from nonideal gas behavior or from the effect of the total pressure on the chemical potential of the solid are neglected in the derivation of (2). The equation is applied here only to the formation of binary hydrates (acid · nH$_2$O); similar equations could be derived for three or more component hydrates.

K_p varies with temperature as

$$RT^2 \frac{d \ln K_p}{dT} = -R \frac{d \ln K_p}{d(1/T)} = v_A H_{f,A}^{0,\text{gas}} + v_B H_{f,B}^{0,\text{gas}} - H_{f,C}^{0,\text{crystal}} = \Delta H_{\text{subl}}^0, \tag{3}$$

where R is the gas constant, the H_f^0s are the standard enthalpies of formation, and ΔH_{subl}^0 is the enthalpy change upon sublimation. The entropy changes, i.e., the intercepts of

$$R \ln K_p = \Delta S_{\text{subl}}^0 - \Delta H_{\text{subl}}^0/T \tag{4}$$

plots, may be found in a similar manner.

Values for H_f^0s and S_f^0s of the pure components at 298.15 K and sometimes directly for the liquid solutions as well, such as for sulfuric acid, are given in standard compilations of thermodynamic data such as *Lide* [1993], *Perry* [1984], *Chase et al.* [1985], *Dean* [1992], etc. For other cases the heat of mixing is added to the sum of the individual heats for the pure liquids to obtain the total heat of formation of the mixture. As the temperature of interest here is not 298.15 K but near 200 K, adjustments are employed where heat capacity data, $C_p(T)$, are available. Since only the difference between the heats of formation between the vapors and the solids is relevant, for convenience, only the components, mixtures, and crystals are adjusted to 200 K and not the elements from which they are formed; that is, rather than H_f^0s, we employ H_fs at 200 K referenced to the elements still at 298.15 K. Thus, to obtain the heat of formation of a hydrate at 200 K, we consider the following cycle: mix the liquids at 298.15 K, cool to melting point, crystallize at the melting point, and further cool to reach 200 K

$$\Delta_f H_{200\text{ K}}(\text{cryst}) = v_A H_{f,A}^{0,\text{liquid}} + v_B H_{f,B}^{0,\text{liquid}} + \Delta_{\text{mix}}^{298.15\text{ K}} H + \int_{298.15\text{ K}}^{T_{\text{fusion}}} Cp(T)\, dT + \Delta_{\text{fusion}}^{T_{\text{fusion}}} H + \int_{T_{\text{fusion}}}^{200\text{ K}} Cp(T)\, dT \tag{5}$$

In addition to the individual compounds (hydrates) we also consider the simultaneous equilibria of pairs of addition compounds (e.g., various hydrates of same molecule, differing only in v_i), which further define the stability regimes of the hydrates. We begin with (1) for one hydrate and introduce

$$v'_A A + v'_B B \Leftrightarrow C' \tag{6}$$

for the other. As the equilibrium partial pressures of B over crystals C and C' are equal, the pair of equations, (2) for K_p and the corresponding equation for K'_p, are combined to eliminate p_B, which yields

$$\left(\frac{v_A}{v_B} - \frac{v'_A}{v'_B}\right) \ln p_A = \frac{1}{v_B} \ln K_p - \frac{1}{v'_B} \ln K'_p, \tag{7}$$

with a temperature dependence

$$-RT^2\left(\frac{v_A}{v_B} - \frac{v'_A}{v'_B}\right) \frac{d \ln p_A}{dT} = \frac{1}{v_B}(H_C^0 - v_A H_A^0 - v_B H_B^0) - \frac{1}{v'_B}(H_{C'}^0 - v'_A H_A^0 - v'_B H_B^0), \tag{8}$$

or equivalently

$$-R \frac{d \ln p_A}{d1/T} = \frac{1}{\dfrac{v_A}{v_B} - \dfrac{v'_A}{v'_B}} \left[\frac{\Delta H_{\text{subl}}^0}{v_B} - \frac{\Delta H'^0_{\text{subl}}}{v'_B}\right] \tag{9}$$

which represents the slope of a $\ln p_A$ versus $1/T$ plot, that is, the equilibrium coexistence line for the two hydrates in question in a phase diagram. A similar equation can be derived for the intercepts (entropy changes).

For the current example of water vapor over a pair of acid hydrates having n and n' water molecules, we substitute $H_2O = A$, acid $= B$, $v_B = v'_B = 1$, $v_A = n$, and $v'_A = n'$ into (9):

$$\frac{d \ln p_{H_2O}}{d(1/T)} = \frac{\Delta H'_{\text{subl}} - \Delta H_{\text{subl}}}{(n - n')R}. \tag{10}$$

Similarly, for acid vapor over the pair we have

$$\frac{d \ln p_{\text{acid}}}{d(1/T)} = \frac{n\Delta H'_{\text{subl}} - n'\Delta H_{\text{subl}}}{(n' - n)R} \tag{11}$$

Experimental Methods

The general experimental methods and procedures used here have been described previously [*Zhang et al.*, 1993a, b], so only brief descriptions will be given here along with any details specific to this work.

Vapor pressures were measured using a static technique in which the samples were held in a glass vessel with the temperature regulated in the range of 180–200 K. Partial pressures were determined with a quadrupole mass spectrometer which had been calibrated for H_2O against pure ice and for HCl against pressures extrapolated from the data of *Fritz and Fuget* [1956]. For experiments involving the HCl hexahydrate, samples had to first be cooled to below 150 K, then warmed to induce nucleation. The estimated errors for these measurements are of the order of ±10%.

Infrared transmission spectra of $HNO_3 \cdot 2H_2O$ were obtained by flattening a drop of the nitric acid solution (63.6 wt %) between silver chloride discs held in a temperature

Table 1. Components at Standard State

Species	H_f^0 298.15 K, kJ mol^{-1}, Liquid	S 298.15 K, J mol^{-1} K^{-1}, Liquid	H_f^0 298.15 K, kJ mol^{-1}, Gas	$\int_{298.15\,K}^{200\,K} Cp\,dT$, kJ mol^{-1}, Gas	H_f 200 K,[a] kJ mol^{-1}, Gas	S 298.15 K, J mol^{-1} K^{-1}, Gas	S 200 K, J mol^{-1} K^{-1}, Gas
H_2O	−285.830 ± .042[b]	69.950 ± .079[b]	−241.826 ± .042[b]	−3.395[c]	−245.221	188.834 ± .042[b]	175.038[c]
HCl	−167.15 ± .1[d,e]	56.5 ± .2[d,f]	−92.31 ± .1[f]	−2.859[c]	−95.169	186.902 ± .005[e]	175.271[c]
HNO_3	−174.18[g]	155.679[g]	−135.13[g]	−4.687[c]	−139.817	266.400[g]	247.468[c]
H_2SO_4	−813.989 ± .67[b]	156.895 ± .08[b]	−735.13 ± 8.4[b]	−7.383[c]	−742.513	298.796 ± 2.1[h]	269.003[c]

Error estimates are given where available for this and other tables.
[a] Referenced to the elements at 298.15 K.
[b] *Chase et al.* [1985].
[c] Using heat capacities from *Chase et al.* [1985].
[d] For dissolving HCl gas in water to ∞ dilution.
[e] *Lide* [1993].
[f] *Dean* [1992].
[g] *Weast* [1984].

controlled cell. Samples were prepared and loaded at room temperature, and spectra were taken at frequent intervals during the temperature cycle. A Nicolet 800 spectrometer with a MCT-A detector was used, scanning at 2 cm^{-1} resolution.

Enthalpies of fusion were measured by differential scanning calorimetry (DSC), using a Perkin-Elmer DSC-7. Titanium or gold plated capsules were used to hold the sample solutions. Calibration of the DSC was made using either ice or cyclohexane. We estimate the uncertainties in the enthalpy measurements to be less than 10%.

Sample solutions were prepared by diluting the concentrated acids with deionized water. The compositions were analyzed by standard acid-base titration or density measurements at room temperature, with an estimated accuracy of ±0.1 wt %. Typically, about 3 cm^3 of liquid were used in the vapor pressure measurements, while the sample volumes for the infrared and thermal analyses were less than 0.03 cm^3.

Results and Discussion

Nitric acid hydrates. For this we use the H_f^0 values given by *Lide* [1993] and the heats of mixing the pure liquids at 298.15 K given by *Forsythe and Giauque* [1942] as well as their heats of fusion and heat capacities. Note that care must be taken to consistently use values from the same source within a given calculation, as enthalpies of formation are much greater than those of vaporization, and hence small differences in H_f^0s would lead to large errors in ΔHs. The standard state values used here are summarized in Table 1.

As mentioned above the temperature of interest here is around 200 K. Vapor phase enthalpies are adjusted from 298.15 K to 200 K via the relation $\Delta_{298.15\,K}^{200\,K} H = \int_{298.15\,K}^{200\,K} C_p\,dT$ using the heat capacity data given by *Chase et al.* [1985]. For the liquid solutions and crystalline hydrates we also use low-order polynomial fits to heat capacity data. On the basis of *Forsythe and Giauque*'s [1942] heat capacity data, as illustrated in Figure 1, we calculate $\int_{298.15\,K}^{T_{fusion}} C_p\,dT$ to be −11.367 kJ mol^{-1} for $HNO_3 \cdot H_2O_{liq}$ and −13.909 kJ mol^{-1} for $HNO_3 \cdot 3H_2O_{liq}$. The value of $\int_{T_{fusion}}^{200\,K} C_p\,dT$ is −2.997 kJ mol^{-1} for $HNO_3 \cdot H_2O_{cryst}$ and −8.464 for $HNO_3 \cdot 3H_2O_{cryst}$. Summing the contributions to (5), we obtain $H_f^{200\,K}$ = −505.45 kJ mol^{-1} for NAM and −1107.6 kJ mol^{-1} for NAT (referenced to the elements at 298.15 K). Table 2 was produced in this manner and Table 3 by a similar process for the entropies.

For $HNO_3 \cdot 2H_2O$ we could not locate temperature dependent heat capacity data below 270 K, so there is greater uncertainty than for nitric acid monohydrate (NAM) and NAT. Liquid phase Cp values were extrapolated from *Timmermans*' [1960] compilation of binary systems properties, and as a rough estimate for crystalline nitric acid dihydrate (NAD) we used a mean of NAM and NAT heat capacities over this temperature range. Using differential scanning calorimetry, we measured the enthalpy change in converting solid NAD at 232 K to liquid solution at 245 K to be −22.546 kJ mol^{-1} from the baseline-corrected integral of the curve in Figure 2 from 232 to 245 K, that is, the combined heat of the peritectic melting of NAD to solution + NAT (the

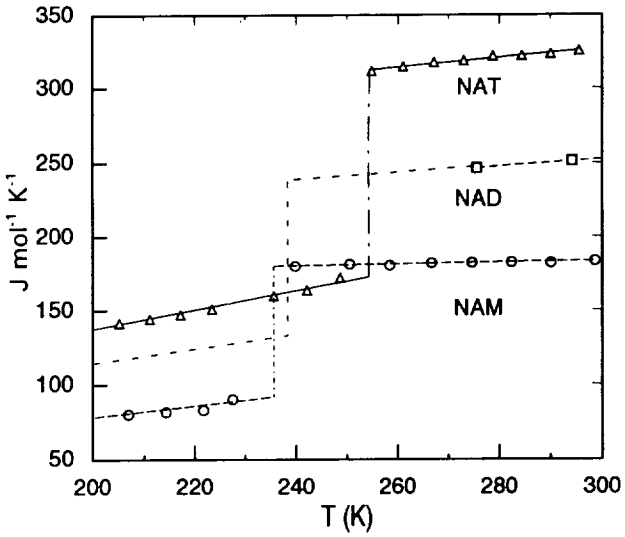

Figure 1. Heat capacity data used for liquid and crystalline $HNO_3 \cdot H_2O$ (NAM), $HNO_3 \cdot 2H_2O$ (NAD), and $HNO_3 \cdot 3H_2O$ (NAT). Symbols for NAM and NAT mark data from *Forsythe and Giauque* [1942]. For the NAD melt, e.g., liquid ~65 wt % HNO_3 aqueous solution, data points are from *Timmermans* [1960], and, as an approximation for crystalline NAD, an intermediate value of NAM and NAT was used.

Table 2. Enthalpies

Species	ΔH_{mixing} 298.15 K From Standard Liquids	H_f^0 298.15 K, Liquid	T_{fusion}, °K	$\int_{298.15}^{T_{fusion}} Cp\,dT$, Liquid	ΔH_{fusion} at T_{fusion}	$\int_{T_{fusion}}^{200} Cp\,dT$, Crystal	H_f 200 K, Crystal[a]	$\Delta H_{subl}^{200\ K}$
H_2O		−285.83 ± .042[b]	273.15	−1.890[c]	−6.011[d]	−2.420[e]	−296.151	−50.93
$HCl \cdot 3H_2O$	+18.67[f]	−1006.0	248.4	−10.2			−1038.0[g]	−207.2[g]
$HCl \cdot 6H_2O$	+9.48[f]	−1872.7	203.2[h]	−38.3[f]	−27.0[i]	~0	−1937.9	−371.4
$HNO_3 \cdot H_2O$	−13.56[j]	−473.57	235.5[j]	−11.4[j]	−17.51[j]	−3.00[j]	−505.45	−120.4
$HNO_3 \cdot 2H_2O$	−20.49[f]	−766.3	238[k]	−14.7[l]	−20.15[m]	−4.4[n]	−805.55	−175.3
$HNO_3 \cdot 3H_2O$	−24.48[j]	−1056.2	254.6[j]	−13.9[j]	−29.11[j]	−8.46[j]	−1107.6	−232.2
$H_2SO_4 \cdot H_2O$	−27.85[c]	−1127.7	281.6[c]	−3.51[o]	−19.93 ± .48[c]	−8.85[b]	−1160.0	−172.2
$H_2SO_4 \cdot 2H_2O$	−43.72[c]	−1429.4	233.7[c]	−16.4[o]	−18.08 ± .16[c]	−4.14[c]	−1468.0	−235.0
$H_2SO_4 \cdot 3H_2O$	−51.88[c]	−1723.4	236.8[c]	−19.3[b]	−23.37 ± .63[c]	−5.79[b]	−1771.9	−293.7
$H_2SO_4 \cdot 4H_2O$	−57.16[c]	−2014.5	244.9[c]	−20.3[o]	−29.73 ± .9[c]	−8.17[c]	−2072.7	−349.3
$H_2SO_4 \cdot 6½H_2O$	−65.28[c]	−2737.2	220.3[c]	−43.1[o]	−33.07 ± 1.1[c]	−5.10[c]	−2818.4	−482.0

Values are in kilojoules per mole.
[a]Referenced to the elements at 298.15 K.
[b]*Chase et al.* [1985].
[c]*Zeleznik* [1991].
[d]*Lide* [1993].
[e]*Giauque and Stout* [1936].
[f]*Weast* [1984].
[g]Using *Hanson and Mauersberger*'s [1990] measurements.
[h]*Vuillard* [1957].
[i]This paper.
[j]*Forsythe and Giauque* [1942].
[k]Metastable, extrapolated from *Ji and Petit* [1991].
[l]*Timmermans* [1960].
[m]This paper, integral from 232 to 245 K minus the heat capacity integrals of NAD from 232 to 238 K and the melt from 238 to 245 K.
[n]Using an intermediate value of NAT and NAM.
[o]*Giauque et al.* [1960].

peak beginning at 232 K) along with the heat of warming and melting the NAT + solution until no NAT remains (the peak ending at 245 K).

Support for the presence of NAD in the calorimetry cell, rather than a NAT + NAM mixture, comes from parallel experiments wherein samples of liquid $HNO_3 \cdot 2H_2O$ solution were held between AgCl windows and cooled and rewarmed as described in the experimental section. As shown in Figure 3, the infrared spectra indicate the spontaneous formation of NAD from the liquid upon cooling and the conversion of NAD to liquid + NAT on warming to the 220–230 K range, followed by the complete melting of NAT by ~245 K. Our spectra compared well with those reported for NAD by *Ritzhaupt and Devlin* [1991] and for NAD and "β" − NAT by *Koehler et al.* [1992]. In addition, the bands in the 2400–2700 cm^{-1} region arising from the incorporation of ~2% heavy water in the sample solutions aided in the identification of the NAD to NAT transition. In some cases, small amounts of NAT formed along with NAD upon cooling, and in these instances, of which Figure 3 is an example, the conversion of NAD to NAT began at lower temperatures than when no NAT formation was observed upon cooling.

Though the actual process in the calorimeter was likely the conversion to NAT followed by its melting, as was observed in the infrared experiments, conversion of the measured $\Delta_{245\ K}^{232\ K} H_{transition}$ value to an approximation for the heat of

Table 3. Entropies

Species	S^0 298.15 K, Liquid	$\int_{298.15\ K}^{T_{fusion}} Cp/T\,dT$, Liquid	$\Delta S_{fusion} = \Delta H_{fusion}/T_{fusion}$	$\int_{T_{fusion}}^{200\ K} Cp/T\,dT$, Crystal	S 200 K, Crystal	Intercept of $R \ln_e K_p$ Versus $1/T$ at 200 K, i.e., ΔS	$\Delta S/R$
H_2O	69.950 ± .079[a]	−6.6202	−22.006	−10.233	31.091	143.95	17.313
$HCl \cdot 3H_2O$		−37.45			136.0[b]	564.4[b]	67.88[b]
$HCl \cdot 6H_2O$		−154.5	−132.8				
$HNO_3 \cdot H_2O$	217.00[c]	−42.78	−74.38	−13.75	86.08	336.4	40.46
$HNO_3 \cdot 2H_2O$	280.2[d]	−55.	−84.6	−20.	120.6	477.0	57.4
$HNO_3 \cdot 3H_2O$	347.15[c]	−50.40	−114.3	−37.23	145.2	627.4	75.46
$H_2SO_4 \cdot H_2O$	211.51[a]	−12.15	−70.77	−36.82	91.78	352.3	42.37
$H_2SO_4 \cdot 2H_2O$	276.363[a]	−61.85	−77.37	−19.09	118.0	501.3	60.26
$H_2SO_4 \cdot 3H_2O$	345.373[a]	−72.58	−98.71	−26.53	147.6	646.5	77.76
$H_2SO_4 \cdot 4H_2O$	414.529[a]	−74.97	−121.4	−36.75	181.4	787.8	94.75
$H_2SO_4 \cdot 6½H_2O$	587.819[a]	−167.1	−150.1	−24.28	246.3	1160	139.5

Values are in J mol^{-1} K^{-1}. $\Delta S/R$ is unitless. Heat capacity integrals use data from same sources as in Table 2.
[a]*Chase et al.* [1985].
[b]Using *Hanson and Mauersberger*'s [1990] measurements.
[c]*Forsythe and Giauque* [1942].
[d]From parameterization of *Clegg and Brimblecombe* [1990].

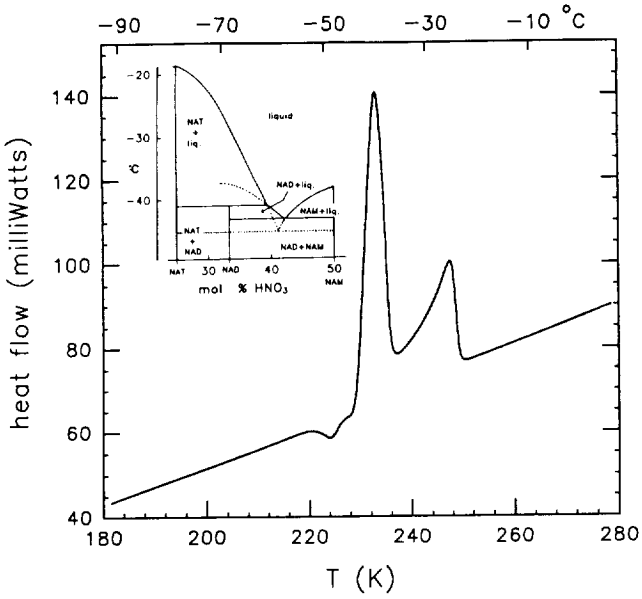

Figure 2. Differential scanning calorimeter (DSC) trace for the conversion $HNO_3 \cdot 2H_2O$ to liquid upon warming. The first peak corresponds to the conversion of NAD to NAT + liquid, and the warmer peak is the melting of the NAT. The inset shows the temperature-composition phase diagram based on the work of *Ji and Petit* [1991], with dashed lines showing extensions of stable phase boundaries into metastable regions.

fusion of NAD at its metastable melting point at 238 K [*Ji and Petit*, 1991] may be done by subtraction of the heat capacity integral of metastable NAD from 232 to 238 K and of the supercooled liquid from 238 to 245 K. This leaves -20.145 kJ mol^{-1} for the (actual or hypothetical) melting of metastable NAD at 238 K. Equation (5) can then be applied to find $\Delta_f H_{200\,K} \approx -805.55$ kJ mol^{-1}.

The slope of a ln K_p versus $1/T$ plot for NAT at 200 K is calculated to be, using (3), $(-232.2$ kJ mol$^{-1})/R = -27930$, which agrees very well with previously reported values. *Worsnop et al.* [1993] measured -28520 ± 470, *Smith* [1990] fit -28100 ± 500 to *Hanson and Mauersberger*'s [1988b] measurements (and also calculated -27000 using a similar analysis to this one but without consideration of the heat capacities), and *Mozurkewich* [1993] calculated -27881 using an analysis which included heat capacity data. For the intercept, $\Delta S/R$, we find a value of 75.46 (with pressure in atmospheres), whereas Worsnop et al. measured 78.7 ± 2.7, Smith obtained 76.52 ± 1, and Mozurkewich 75.32.

For nitric acid monohydrate we arrive at $\ln K_p = 40.46 - 14480/T$, which may be compared with $\ln K_p = (44.3 \pm 1) - (15330 \pm 500)/T$ from *Smith*'s [1990] analysis and $\ln K_p = (44.1 \pm 1.7) - (15264 \pm 300)/T$ from *Worsnop et al.*'s [1993] observations. And for the dihydrate we obtain $\ln K_p = 57.4 - 21163/T$, which can be compared to Worsnop et al.'s $\ln K_p = (64.9 \pm 2.2) - (22630 \pm 360)/T$.

The slope of $\ln p_{H_2O}$ versus $1/T$ at the NAT-NAM coexistence, that is, the right hand side of (10), is calculated to be $(-55860$ J mol$^{-1})/R$. For convenience, in comparison to a $\log_{10} p_{H_2O} = A + B/T$ plot, we have $B = -55860/(R \ln_e 10) = -2918$, which agrees well with *Hanson and Mauersberger*'s [1988b] measured value of -2819. Using (11), we estimate $B = -3370$ for the slope of a $\log_{10} p_{HNO_3} = A + B/T$ plot, which again agrees well with *Hanson and Mauersberger*'s [1988b] value of -3561. Other coexistence slopes are given in Table 4.

Hydrates of hydrochloric acid. The table entries are calculated in the same manner as for the nitric acid hydrates.

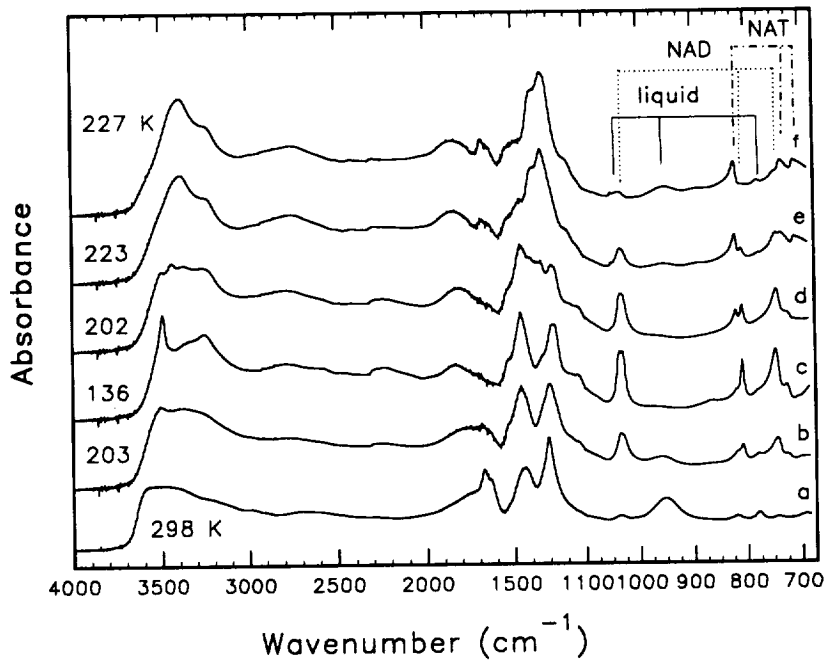

Figure 3. Infrared spectra taken through cycle of cooling and warming $HNO_3 \cdot 2H_2O$. This sample spontaneously crystallized to form the crystalline dihydrate upon cooling from 298 K to 203 K (traces a and b), and gradually converted to a trihydrate + liquid mixture upon warming to 227 K (traces c through f).

Table 4. Coexistence Line Slopes at 200 K

Coexistence Pair	Calculated Slope of $\log_{10} p_{H_2O}$ Versus $1/T$	Experimental Slope of $\log_{10} p_{H_2O}$ Versus $1/T$	Calculated Slope of $\log_{10} p_{acid}$ Versus $1/T$	Experiment Slope of $\log_{10} p_{acid}$ Versus $1/T$
ice:$HCl \cdot 6H_2O$	−2660[a]		−3440	−3340[b]
ice:$HNO_3 \cdot 3H_2O$	−2660[a]		−4145	−3968[c]
ice:$H_2SO_4 \cdot 4H_2O$	−2660[a]		−7600	
ice:$H_2SO_4 \cdot 6½ H_2O$	−2660[a]		−7880	
$HCl \cdot 3H_2O$:$HCl \cdot 6H_2O$	−2860		−2250	
$HNO_3 \cdot H_2O$:$HNO_3 \cdot 2H_2O$	−2870		−3420	
$HNO_3 \cdot H_2O$:$HNO_3 \cdot 3H_2O$	−2918	−2819[c]	−3370	−3561[c]
$HNO_3 \cdot 2H_2O$:$HNO_3 \cdot 3H_2O$	−2970		−3215	
$H_2SO_4 \cdot H_2O$:$H_2SO_4 \cdot 2H_2O$	−3280		−5720	
$H_2SO_4 \cdot 2H_2O$:$H_2SO_4 \cdot 4H_2O$	−2985	−3236[d]	−6310	
$H_2SO_4 \cdot 4H_2O$:$H_2SO_4 \cdot 6½ H_2O$	−2770		−7155	

[a] Same as ice from assumption of pure crystal (Raoult's Law).
[b] This paper.
[c] *Hanson and Mauersberger* [1988b].
[d] *Zhang et al.* [1993b].

The heat of vaporization of the trihydrate is estimated from the vapor pressure measurements of *Hanson and Mauersberger* [1990]. The hexahydrate heat of fusion, −26.98 kJ mol^{-1}, was measured in our laboratory using differential scanning calorimetry, as for NAD.

A plot of the HCl partial pressure over the HCl/H_2O system is presented in Figure 4. Vapor pressures over liquid solutions, extrapolated from *Fritz and Fuget* [1956], are shown as long dashed lines; the shorter dashed lines indicate where the vapor pressures of the liquids and solids are equal (ice, $HCl \cdot 3H_2O$ or $HCl \cdot 6H_2O$), i.e., the freezing envelopes; and the solid line defines the trihydrate-hexahydrate boundary based on measurements by *Hanson and Mauersberger* [1990]. The triangles mark our measurements of p_{HCl} over ice-liquid equilibrium mixtures, and the pluses are for ice-hexahydrate coexistence mixtures. We find excellent agreement between observed vapor pressures and those predicted using (11), shown as the dotted line in the figure, along the ice-hexahydrate coexistence line.

Hydrates of sulfuric acid. Here the individual values for the K_p are of less interest because solid-vapor equilibria are unlikely to be maintained at the extremely low ambient mixing ratios of H_2SO_4 vapor, but the water vapor pressures over coexisting solids are of importance. As water pressures over ice-hydrate coexistence systems are negligibly different from those of ice alone (from the fact that the ice phase is very nearly pure), calculated and measured values only over the tetrahydrate-dihydrate coexistence mixture are presented in Figure 5.

Stratospheric Implications

Phase diagrams presenting vapor pressures as a function of temperature (such as those shown in Figures 4 and 5) can be used to place constraints on the existence of various solid phases in the stratosphere. Consider a particular acid hydrate: it is stable against evaporation only if its water and acid vapor pressures are equal or smaller than the corresponding environmental partial pressures. It was in this way that the formation of NAT clouds in the stratosphere at temperatures above the ice frost point was first predicted [*Toon et al.*, 1986; *Crutzen and Arnold*, 1986].

On the other hand, stability does not necessarily imply formation; nucleation needs to take place first if a condensed phase is to form from vapor or if a solid phase is to form from a liquid or from another solid. (Note, however, that under conditions such as those applicable to the atmosphere,

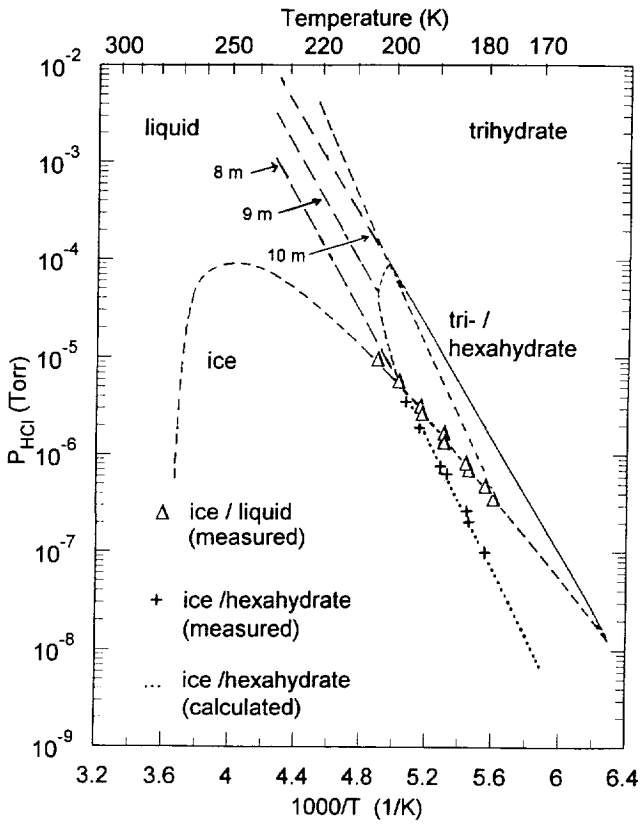

Figure 4. Plot of log P_{HCl} versus $1000/T$. As discussed in the text, the long dashed lines are for liquid solutions, with the concentrations in molal units labeled; the shorter dashed lines represent the freezing envelopes; and the solid line defines the trihydrate-hexahydrate boundary. Triangles mark our measurements of p_{HCl} over ice-liquid equilibrium mixtures, and the pluses are for ice-hexahydrate coexistence mixtures. The dotted line is calculated from (11).

melting, evaporation, and sublimation always occur practically at equilibrium.) This behavior leads to some nonequilibrium situations where phase diagrams are still useful, namely in terms of the stability of metastable phases. An example from Figure 4 is HCl hexahydrate: it nucleates only from the liquid supercooled to below ~170 K [*Vuillard*, 1957; *Abbatt et al.*, 1992]. Hence a practical phase diagram for a HCl/H_2O system that has not experienced temperatures below ~170 K (e.g., droplets in the stratosphere) is one in which the hexahydrate is absent; it contains regions in which the liquid, ice, or the trihydrate are metastable with respect to the hexahydrate, and yet valid predictions of melting, evaporation, and/or sublimation of the various phases can be made with a diagram that ignores the hexahydrate, even if they are metastable with respect to the hexahydrate. Thus Figure 4 shows that unless some efficient nuclei for the hexahydrate are present, no HCl hydrates are expected to form in the stratosphere, as HCl partial pressures do not exceed 10^{-6} torr and temperatures never fall to 170 K.

Metastability commonly arises in solid-solid phase transformations: if equilibrium is strictly maintained, as temperature and partial pressures change, a solid phase transforms into a second one when their coexistence line (i.e., as given by (10) and (11) for hydrates) is crossed. However, if nuclei for the second solid phase are absent and do not form readily, the first phase persists into the region of stability of the second one, until the first solid either evaporates or melts, depending on the partial pressure-temperature constraints. Melting occurs under conditions represented by an extension of the freezing envelope of the first solid into the region of stability of the second one.

We have been able to observe in the laboratory various types of metastable phase behavior, as expected from the phase diagrams. For example, ice melts in the presence of HCl vapor at temperatures well below the eutectic (as illustrated in Figure 4 by the extension of the ice melting curve, the short dashes, past the intersection with the HCl trihydrate curve); neither the HCl hexahydrate nor the trihydrate forms readily from ice [*Abbatt et al.*, 1992]. Similarly, when warming sulfuric acid tetrahydrate with the water partial pressure maintained at 4×10^{-4} torr, the tetrahydrate is not observed to transform into crystalline dihydrate along the $H_2SO_4 \cdot 4H_2O$:$H_2SO_4 \cdot 2H_2O$ coexistence curve at ~217 K but is observed to become liquid at a slightly warmer temperature where the extended $H_2SO_4 \cdot 4H_2O$:liquid curve is intersected [*Zhang et al.*, 1993b; *Middlebrook et al.*, 1993]. On the other hand, if the two solid phases are initially present, it is possible to determine experimentally their coexistence line, for example, by changing temperature and simultaneously measuring the vapor pressures, provided, of course, that the timescale of the measurements is long enough for equilibrium to be maintained. It is in this fashion that the various coexistence lines described above were experimentally examined. Similarly, metastable phase boundaries are experimentally accessible by carrying out measurements in the absence of the appropriate nuclei and in the direction of equilibrium transformations, e.g., melting.

Concluding Remarks

The thermodynamic properties relating to vapor pressures of the acid/water binary systems important in the chemistry of the stratosphere are now known fairly well, especially for the nitric and sulfuric acid systems. In addition to determinations of whether a given hydrate will be stable under certain conditions, accurate values for the equilibrium constants Kp's are also necessary for calculating the rates of heterogeneous reactions occurring on the particle surfaces, as rates of reactions such as $ClONO_2 + HCl \rightarrow Cl_2 + HNO_3$ have been found to be highly dependent upon the water vapor pressure of the hydrate [*Abbatt and Molina*, 1992; *Chu et al.*, 1993; *Hanson and Ravishankara*, 1993].

We conclude from this analysis that the Kp's of the individual hydrates as well as the vapor pressures over coexisting pairs of hydrates which have been measured are in good agreement with values calculated using thermodynamic relationships.

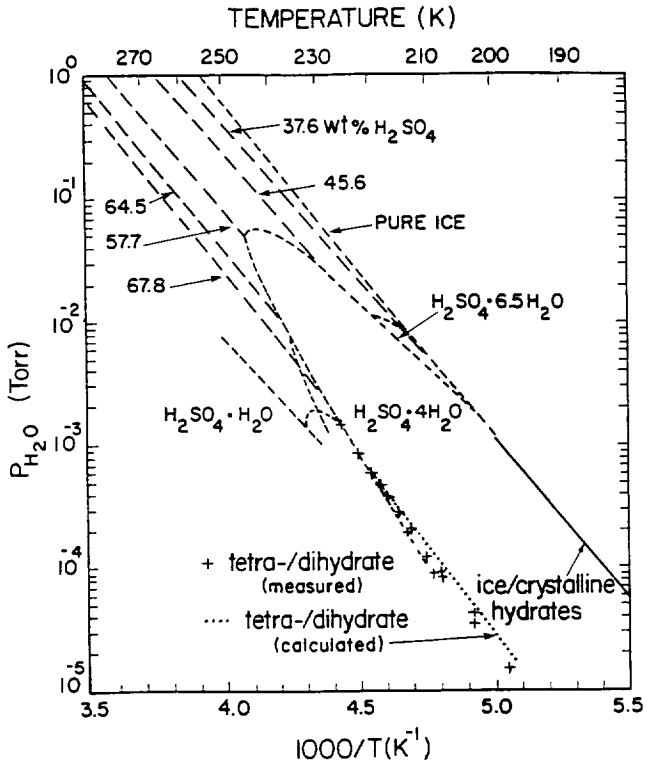

Figure 5. As in Figure 4 but for p_{H_2O} over the H_2SO_4/H_2O system. The coexistence line is calculated from (10) and data points are from *Zhang et al.* [1993b].

Acknowledgments. This research was supported by an NSF grant (ATM-9017150) and a NASA grant (NAG2-632) to the Massachusetts Institute of Technology. R. Z. was supported by a NASA graduate fellowship.

References

Abbatt, J. P. D., and M. J. Molina, Heterogeneous interactions of $ClONO_2$ and HCl on nitric acid trihydrate at 200 K, *J. Phys. Chem.*, *96*, 7674–7679, 1992.

Abbatt, J. P. D., K. D. Beyer, A. F. Fucaloro, J. R. McMahon, P. J. Wooldridge, R. Zhang, and M. J. Molina, Interactions of HCl vapor with water ice: Implications for the stratospheric, *J. Geophys. Res.*, *97*, 15,819–15,826, 1992.

Beyer, K. D., S. W. Seago, H. Y. Chang, and M. J. Molina, Composition and freezing of aqueous H_2SO_4/HNO_3 solutions

under polar stratospheric conditions, *Geophys. Res. Lett.*, *21*, 871–874, 1994.

Cady, G. H., and J. H. Hildebrand, Freezing points of the system water-hydrogen fluoride, *J. Am. Chem. Soc.*, *52*, 3843–3846, 1930.

Chase, M. W., Jr., C. A. Davies, J. R. Downey, D. J. Frurip, R. A. McDonald, and A. N. Syverud, *JANAF Thermochemical Tables*, 3rd ed., American Chemical Society, New York, 1985.

Chu, L. T., M.-T. Leu, and L. F. Keyser, Heterogeneous reactions of HOCl + HCl → Cl_2 + H_2O and $ClONO_2$ + HCl → Cl_2 + HNO_3 on ice surfaces at polar stratospheric conditions, *J. Phys. Chem.*, *97*, 12,798–12,804, 1993.

Clegg, S. L., and P. Brimblecombe, Equilibrium partial pressures and mean active and osmotic coefficients of 0–100% nitric acid as a function of temperature, *J. Phys. Chem.*, *94*, 5369–5380, 1990.

Crutzen, P. J., and F. Arnold, Nitric acid cloud formation in the cold Antarctic stratosphere: A major cause for the springtime ozone hole, *Nature*, *324*, 651–655, 1986.

Dean, J. A., *Lange's Handbook of Chemistry*, McGraw-Hill, New York, 1992.

Denbigh, K., *The Principles of Chemical Equilibrium*, Cambridge University Press, New York, 1981.

Forsythe, W. R., and W. F. Giauque, The entropies of nitric acid and its mono- and tri-hydrates. Their heat capacities from 15 to 300 K. The heats of dilution at 298.15 K. The internal rotation and free energy of nitric acid gas. The partial pressures over its aqueous solutions, *J. Am. Chem. Soc.*, *64*, 48–61, 1942.

Fritz, J. J., and C. R. Fuget, Vapor pressures of aqueous hydrogen chloride solutions, 0 to 50°C, *Chem. Eng. Data Ser.*, *1*, 10–12, 1956.

Giauque, W. F., and J. W. Stout, The entropy of water and the third law of thermodynamics. The heat capacity of ice from 15 to 273 K, *J. Am. Chem. Soc.*, *58*, 1144–1150, 1936.

Giauque, W. F., E. W. Hornung, J. E. Kunzler, and T. R. Rubin, The thermodynamic properties of aqueous sulfuric acid solutions and hydrates from 15 to 300 K, *J. Am. Chem. Soc.*, *82*, 62–70, 1960.

Hanson, D., and K. Mauersberger, Vapor pressures of HNO_3/H_2O solutions at low temperatures, *J. Phys. Chem.*, *92*, 6167–6170, 1988a.

Hanson, D., and K. Mauersberger, Laboratory studies of the nitric acid trihydrate: Implications for the south polar stratosphere, *Geophys. Res. Lett.*, *15*, 855–858, 1988b.

Hanson, D., and K. Mauersberger, H_2O/HCl solid-phase vapor pressures and HCl solubility in ice, *J. Phys. Chem.*, *94*, 4700–4705, 1990.

Hanson, D., and A. Ravishankara, The reaction $ClONO_2$ + HCl on NAT, NAD, and frozen sulfuric acid and the hydrolysis of N_2O_5 and $ClONO_2$ on frozen sulfuric acid, *J. Geophys. Res.*, *98*, 22,931–22,936, 1993.

Ji, K., and J.-C. Petit, The HNO_3-H_2O phase diagram revisited in the temperature and concentration ranges of PSC formation, paper presented at the CEC/EUROTRAC Discussion Meeting on Multiphase Processes of Atmospheric Interest, Royal Society of Chemistry, York, England, September, 1991.

Koehler, B. G., A. M. Middlebrook, and M. Tolbert, Characterization of model polar stratospheric cloud films using Fourier transform infrared spectroscopy and temperature programed desorption, *J. Geophys. Res.*, *97*, 8065–8074, 1992.

Kolb, C. E., et al., Laboratory studies of atmospheric heterogeneous chemistry, in *Current Problems and Progress in Atmospheric Chemistry*, edited by J. R. Barker, World Scientific, Singapore, in press, 1995.

Lide, D. R. (Ed.), *CRC Handbook of Chemistry and Physics*, CRC Press, Boca Raton, Fla., 1993.

McElroy, M. B., R. J. Salawitch, S. C. Wofsy, and J. A. Logan, Reduction of Antarctic ozone due to synergistic interactions of chlorine and bromine, *Nature*, *321*, 759–762, 1986.

Middlebrook, A. M., L. T. Iraci, L. S. McNeill, B. G. Koehler, M. A. Wilson, O. W. Saastad, M. A. Tolbert, and D. Hanson, Fourier transform infrared studies of thin H_2SO_4/H_2O films: Formation, water uptake, and solid-liquid phase changes, *J. Geophys. Res.*, *98*, 20,473–20,481, 1993.

Molina, M. J., Heterogeneous chemistry on polar stratospheric clouds, *Atmos. Environ.*, Part A, *25*, 2535–2537, 1991.

Molina, M. J., The probable role of stratospheric "ice" clouds: Heterogeneous chemistry of the "Ozone Hole," in *The Chemistry of the Atmosphere: Its Impact on Global Change*, edited by J. G. Calvert, pp. 27–38, Blackwell Scientific, Boston, Mass., 1994.

Molina, M. J., R. Zhang, P. J. Wooldridge, J. R. McMahon, J. E. Kim, H. Y. Chang, and K. Beyer, Physical chemistry of the $H_2SO_4/HNO_3/H_2O$ system: Implication for the formation of polar stratospheric clouds and heterogeneous chemistry, *Science*, *261*, 1418–1423, 1993.

Mozurkewich, M., Effect of competitive adsorption on polar stratospheric cloud reactions, *Geophys. Res. Lett.*, *20*, 355–358, 1993.

Perry, R. H. (Ed.), *Chemical Engineer's Handbook*, McGraw-Hill, New York, 1984.

Ritzhaupt, G., and J. P. Devlin, Infrared spectra of nitric and hydrochloric acid-hydrate thin films, *J. Phys. Chem.*, *90*, 90–95, 1991.

Smith, R. H., Formation of nitric acid hydrates: A chemical equilibrium approach, *Geophys. Res. Lett.*, *17*, 1291–1294, 1990.

Solomon, S., The mystery of the ozone "hole," *Rev. Geophys.*, *26*, 131–148, 1988.

Timmermans, J., *The Physico-Chemical Constants of Binary Systems in Concentrated Solutions*, Wiley-Interscience, New York, 1960.

Toon, O. B., P. Hamill, R. P. Turco, and J. Pinto, Condensation of HNO_3 and HCl in the winter polar stratospheres, *Geophys. Res. Lett.*, *13*, 1284–1287, 1986.

Turco, R. P., R. C. Whitten, and O. B. Toon, Stratospheric aerosols: Observations and theory, *Rev. Geophys.*, *20*, 233–279, 1982.

Vuillard, G. C., Contribution a l'étude de l'état vitreux et de la cristallisation des solutions aqueuses, *Ann. Chim. Paris*, *13*, 233–297, 1957.

Weast, R. C. (Ed.), *CRC Handbook*, CRC Press, Boca Raton, Fla., 1984.

Worsnop, D. R., L. E. Fox, M. S. Zahniser, and S. C. Wofsy, Vapor pressures of solid hydrates of nitric acid: Implications for polar stratospheric clouds, *Science*, *259*, 71–74, 1993.

Zeleznik, F. Thermodynamic properties of the aqueous sulfuric acid system to 350 K, *J. Phys. Chem. Ref. Data*, *20*, 1157–1200, 1991.

Zhang, R., P. J. Wooldridge, and M. J. Molina, Vapor pressure measurements for the $H_2SO_4/HNO_3/H_2O$ and H_2SO_4/HCl/H_2O systems: Incorporation of stratospheric acids into background sulfate aerosols, *J. Phys. Chem.*, *97*, 8541–8548, 1993a.

Zhang, R., P. J. Wooldridge, J. P. D. Abbatt, and M. J. Molina, Physical chemistry of the H_2SO_4/H_2O binary system at low temperature: Stratospheric implications, *J. Phys. Chem.*, *97*, 7351–7358, 1993b.

Zhang, R., J. T. Jayne, and M. J. Molina, Heterogeneous interactions of $ClONO_2$ and HCl with sulfuric acid tetrahydrate: Implication of the stratosphere, *J. Phys. Chem.*, *98*, 867–874, 1994.

M. J. Molina and P. J. Wooldridge, Massachusetts Institute of Technology, Department of Earth, Atmospheric and Planetary Sciences, Department of Chemistry, Room 54-1320, Cambridge, MA 02139.

R. Zhang, Jet Propulsion Laboratory, California Institute of Technology, 4800 Oak Grove Drive, Pasadena, CA 91109.

(Received February 11, 1994; revised September 29, 1994; accepted October 13, 1994.)